ACS APPLIED MATERIALS & INTERFACES

Research Article

www.acsami.org

Single-Composition Trichromatic White-Emitting $Ca_4Y_6(SiO_4)_6O$: $Ce^{3+}/Mn^{2+}/Tb^{3+}$ Phosphor: Luminescence and Energy Transfer

Guogang Li,[†,‡] Yang Zhang,[†,‡] Dongling Geng,[†,‡] Mengmeng Shang,[†,‡] Chong Peng,[†,‡] Ziyong Cheng,[†] and Jun Lin*[,†]

[†]State Key Laboratory of Rare Earth Resource Utilization, Changchun Institute of Applied Chemistry, Chinese Academy of Sciences, Changchun 130022, P. R. China

[‡]Graduate School of the Chinese Academy of Sciences, Beijing 100049, P. R. China

Supporting Information

ABSTRACT: A series of $Ca_4Y_6(SiO_4)_6O$ (CYS): $Ce^{3+}/Mn^{2+}/Tb^{3+}$ oxyapatite phosphors were prepared via high-temperature solid-state reaction. Under UV excitation, there exist dual energy transfers (ET), i.e., $Ce^{3+}\rightarrow Mn^{2+}$ and $Ce^{3+}\rightarrow Tb^{3+}$ in the CYS: Ce^{3+}, Mn^{2+}, Tb^{3+} system and their emitting colors can be adjusted from blue to orange-red via ET of $Ce^{3+}\rightarrow Mn^{2+}$ and from blue to green via ET of $Ce^{3+}\rightarrow Tb^{3+}$, respectively. Moreover, a wide-range-tunable white light emission with high quantum yields (13%-30%) were obtained by precisely controlling the contents of Ce^{3+}, Mn^{2+} and Tb^{3+} ions. On the other hand, the CL properties of CYS: Ce^{3+}, Mn^{2+}, Tb^{3+} phosphors have been investigated in detail. The studied results indicate that the as-prepared CYS: Ce^{3+}, Mn^{2+}, Tb^{3+} phosphors have good CL intensity and CIE color coordinate stability with a color-tunable emission crossing the whole white light region under low-voltage electron beam excitation. In general, the white light with varied hues has been obtained in Ce^{3+}, Mn^{2+}, and Tb^{3+}-triactivated CYS phosphors by utilizing the principle of energy transfer and properly designed activator contents under UV (284, 358 nm) and low-voltage (1−5 kV) electron beam excitation, which make them as a potential single-composition trichromatic white-emitting phosphor.

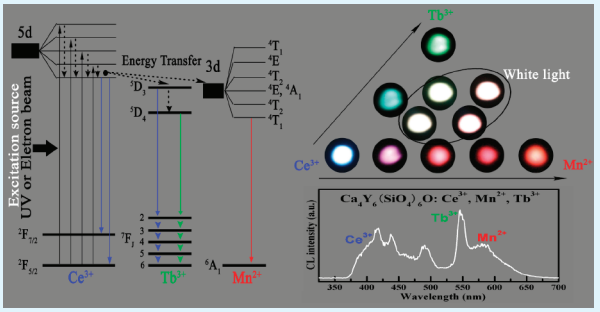

KEYWORDS: *oxyapatite, rare earth ion, Mn^{2+}, energy transfer, white emission, cathodoluminescence*

1. INTRODUCTION

In recent years, there is a growing interest in generation of white light sources for a range of applications, such as solid-state lighting, multicolor three-dimensional display, back light, and so on.[1−5] To date, many efforts have been made to obtain white light emission with a high color rendering index using phosphors to convert ultraviolet (UV), blue, or infrared light into a combination of RGB.[6−8] However, in the three-converter (RGB) system, the manufacture cost is high and the blue emission efficiency is poor because of the strong reabsorption of blue light by the red, green-emitting phosphors. To circumvent these disadvantages, researchers are turning their attention to the investigation of efficient, durable, and single-phase white-light-emitting phosphors with RGB components through energy transfer between activators.[9,10] It is well-known that energy transfer plays an important role in the optical properties of luminescent materials both from theoretical and practical points of view. Rare earth ions have been playing an important role in modern lighting and display fields due to the abundant emission colors based on their 4f → 4f or 5d → 4f transitions.[11] The Ce^{3+} with the $4f^1$ configuration in solids shows efficient broad band luminescence due to the 4f−5d parity allowed electric dipole transition. The Ce^{3+} ion has a larger Stokes shift than those of the other rare earth ions, because of the extended radial wave functions of the 5d state. Furthermore, the Ce^{3+} ion can also act as an efficient sensitizer by transferring a better part of its excitation energy to coactivators.[12] The trivalent Tb^{3+} are generally used as an green emitting activator, whose emission is mainly due to transitions of $^5D_3 \rightarrow {}^7F_J$ in the blue region and $^5D_4 \rightarrow {}^7F_J$ in the green region (J = 6, 5, 4, 3, 2) depending on its doping concentration.[13] The transition metal ion Mn^{2+} can give a broad band emission in the visible range owing to the forbidden d−d transition, and the emission color of Mn^{2+} can vary from green to red depending on the crystal field.[14,15] Because the d−d transition of Mn^{2+} is forbidden and difficult to pump, the emission of Mn^{2+} ions is generally excited by energy transfer from the host or the sensitizer. So far, the $Ce^{3+}\rightarrow Mn^{2+}$ energy transfer mechanism has been investigated in many inorganic hosts, such as fluorides,[16,17] phosphates,[18] and borates,[9] whereas the $Ce^{3+}\rightarrow Tb^{3+}$ energy transfer has been extensively reported.[19−21] In these systems, there is a common feature that

Received: September 28, 2011
Accepted: December 3, 2011
Published: December 3, 2011

Ce^{3+} and Mn^{2+}/Tb^{3+} ions simultaneously substitute one or two lattice sites and the Ce^{3+} ions serve as effective sensitizer ions for Mn^{2+} or Tb^{3+}, transferring the energy from the 5D level of the Ce^{3+} to the 4G level of the Mn^{2+} or to the $^5D_{3,4}$ level of Tb^{3+} by a process of resonance transfer via a spin exchange mechanism, which not only help Mn^{2+} and Tb^{3+} ions to emit efficiently but also tune their emission colors from blue to orange/red and from blue to green, respectively. Furthermore, a single-phase white-light-emitting phosphor utilizing energy transfer can avoid the reabsorption for blue or UV light by the red-/green emitting phosphors and the mixing of RGB phosphors. Consequently, it can enhance the luminescence efficiency and color reproducibility of the white light source and reduce manufacturing costs.

On the other hand, the field-emission displays (FEDs) have been considered as one of the most promising next-generation flat panel displays because of their potential to provide displays with thin panels, self-emission, wide viewing, quick response time, high brightness, high contrast ratio, lightweight, and low power consumption. To realize the full-color FEDs, it is necessary to develop some novel phosphors with good stability and high efficiency as well as color-tunable emission.[22−25] Single-phased phosphors with multicolor-tunable emission via energy transfer are good candidates for this application in FEDs. Rare-earth and transitional-metal-doped, oxide-based phosphors for FEDs have been of great interest due to their excellent light output, color-rendering properties, and superior stability under electron bombardment.[22−25]

The compounds with oxyapatite structure that represent excellent thermal and chemical stability as well as the stabilization of ionic charge have testified their efficiency as luminescent hosts. Among the many synthetic oxyapatites, the ternary rare-earth-metal silicate $Ca_4Y_6(SiO_4)_6O$ (CYS) is an efficient host lattice for the luminescence of various rare earth ions and mercury-like ions.[26,27] This oxyapatite host lattice consists of two cationic sites, that is, the 9-fold coordinated 4*f* sites with C_3 point symmetry and 7-fold coordinated 6*h* sites with C_s point symmetry.[28,29] Both sites are suitable and easily accommodate a great variety of rare earth and transitional-metal ions. To the best of our knowledge, there are only several reports about rare earth ions-doped CYS phosphors so far and rare reports have been found on the detailed photoluminescence (PL) properties of Mn^{2+} and the sensitization effect of Ce^{3+} to Mn^{2+} in the CYS host lattice.[26,27] Moreover, the dual energy transfer induced multicolor-tunable (including white light) emission of CYS: Ce^{3+}, Mn^{2+}, Tb^{3+} phosphors has not been reported. In addition, the cathodoluminescence (CL) properties of Ce^{3+}, Mn^{2+}, Tb^{3+}-activated CYS phosphors have also not been investigated. Herein, we reported the synthesis of CYS: $Ce^{3+}/Mn^{2+}/Tb^{3+}$ phosphors using solid state reaction. The energy transfer properties from Ce^{3+} to Mn^{2+} and from Ce^{3+} to Tb^{3+} were investigated and the critical distance (R_C) of $Ce^{3+}\rightarrow Mn^{2+}$ in CYS host was calculated. The chromaticity-tunable luminescence including white light in the CYS: Ce^{3+}, Mn^{2+}, Tb^{3+} phosphors was obtained by varying the relative doping concentrations of Ce^{3+}, Mn^{2+} and Tb^{3+}. Moreover, the CL properties of CYS: $Ce^{3+}/Mn^{2+}/Tb^{3+}$ phosphors were also investigated in detail.

2. EXPERIMENTAL SECTION

Preparation. A series of $Ca_4Y_6(SiO_4)_6O$: x mol % Ce^{3+}, y mol % Mn^{2+}, z mol % Tb^{3+} (abbreviated as CYS: x mol % Ce^{3+}, y mol % Mn^{2+}, z mol % Tb^{3+}; Ce^{3+}/Tb^{3+}, and Mn^{2+} substitute of Y^{3+} and Ca^{2+}, respectively) powder samples were prepared by high temperature solid state reaction process. The doping concentrations of Ce^{3+}, Mn^{2+} and Tb^{3+} were chosen as 1−20 mol % of Ce^{3+}, 0.5−8 mol % of Mn^{2+} and 1−8 mol % of Tb^{3+} in $Ca_4Y_6(SiO_4)_6O$, respectively. Typically, stoichiometric amounts of $CaCO_3$ (Aldrich, 99.99%), SiO_2 (Aldrich, 99.99%), Y_2O_3, CeO_2, Tb_4O_7 (all 99.99%, Shin-Etsu Chemical Co. Ltd., Tokyo, Japan), and $MnCO_3$ (Aldrich, 99.99%) were thoroughly mixed in an agate mortar for 1 h with an appropriate amount of ethanol and then dried at 90 °C for 2 h. The powder mixtures were sintered at 1350 °C for 2 h in a reducing atmosphere of H_2 (5%) and N_2 (95%) to produce the final samples.

Characterization. The X-ray diffraction (XRD) patterns were performed on a D8 Focus diffractometer at a scanning rate of 10° min^{-1} in the 2θ range from 15° to 70° with graphite-monochromatized Cu $K\alpha$ radiation (λ = 0.15405 nm). The photoluminescence (PL) measurements were recorded with a Hitachi F-7000 spectrophotometer equipped with a 150 W xenon lamp as the excitation source. The cathodoluminescence (CL) measurements were conducted in an ultrahigh-vacuum chamber (<1 × 10^{-8} Torr), where the phosphors were excited by an electron beam at a voltage range of 1−5 kV with different filament currents 80−95 mA, and the spectra were recorded using an F-7000 spectrophotometer. Photoluminescence Quantum Yield (QY) was measured by absolute PL quantum yield measurement system C9920−02. The luminescence decay lifetime were obtained from a Lecroy Wave Runner 6100 Digital Osilloscope (1 GHz) using a tunable laser (pulse width = 4 ns, gate = 50 ns) as the excitation (Continuum Sunlite OPO). All the measurements were performed at room temperature (RT).

3. RESULTS AND DISCUSSION

Structure. The composition and phase purity of the as-prepared powder samples were first examined by XRD. Figure 1 shows the representative XRD patterns of as-prepared Ce^{3+}, Mn^{2+}, Tb^{3+} ions doped CYS samples, for example, CYS: 10 mol % Ce^{3+}, CYS: 10 mol % Ce^{3+}, 3 mol % Mn^{2+}, CYS: 10 mol % Ce^{3+}, 5 mol % Tb^{3+} and CYS: 10 mol % Ce^{3+}, 3 mol % Mn^{2+}, 2 mol % Tb^{3+} samples annealed at 1350 °C for 2 h. It is obvious that the diffraction peaks of all these samples can be exactly assigned to pure hexagonal phase of $Ca_4Y_6(SiO_4)_6O$ [space group: $P6_3/m$ (176)]

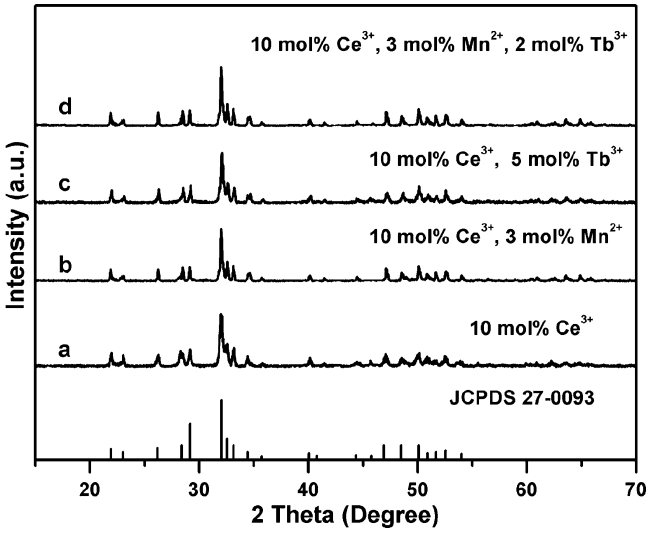

Figure 1. XRD patterns of (a) CYS: 10 mol % Ce^{3+}, (b) CYS: 10 mol % Ce^{3+}, 3 mol % Mn^{2+}, (c) CYS: 10 mol % Ce^{3+}, 5 mol % Tb^{3+} and (d) CYS: 10 mol % Ce^{3+}, 3 mol % Mn^{2+}, 2 mol % Tb^{3+} samples sintered at 1350 °C for 2 h in the N_2/H_2 = 95%/5% atmosphere. The standard data for $Ca_4Y_6(SiO_4)_6O$ (JCPDS No.27−0093) is shown as reference.

according to JCPDS file 27−0093, indicating that the Ce^{3+}, Mn^{2+} and Tb^{3+} ions were completely dissolved in the $Ca_4Y_6(SiO_4)_6O$ host lattice at current doping concentration without inducing significant changes in the crystal structure. The ternary rare-earth-metal silicate $Ca_4Y_6(SiO_4)_6O$ is isostructural to natural oxyapatite $Ca_{10}(PO_4)_6F_2$, which has a hexagonal space group $P6_3/m$ and cell parameters of a = 9.356 Å, c = 6.793 Å, V = 514.96 Å^3, Z = 1, and its crystal structure is shown in Figure S1 (Supporting Information). The crystal structure of CYS indicates that the cations located at 4*f* site and its surrounding nine oxygen atoms forms a tetrakaidecahedra, and these tetrakaidecahedra connect each other by tetrahedral SiO_4 groups.[30] While the cations located at 6*h* sites form decahedra with its surrounding seven oxygen atoms, and these decahedra connect each other through sharing plane, edge and vertex.[30] Finally, the tetrakaidecahedra and decahedra are connected through tetrahedral SiO_4 groups and through sharing plane, edge and vertex. As suggested by G. Blasse,[31] the most prominent structural characteristic of CYS crystal structure is Ca^{2+} ions occupy the four 4*f* (C_3) sites with nine coordination, whereas Y^{3+} ions occupy the six 6*h* (C_3) sites with seven coordination. Moreover, the 4*f* site with nine-coordination in oxyapatite structure needs large cations for its space, whereas the 6*h* site with seven-coordination is favorable for high charge cations because of the fact that it has a O(4) ion to coordinate.[32] The Ce^{3+} has a larger ionic radius (1.196 Å for CN = 9) and higher charge (+3), which are favorable for 4*f* site and 6*h* sites, respectively. Therefore the Ce^{3+} ions simultaneously occupy the 4*f* site and 6*h* site in oxyapatite structure. The same situation is similar to Tb^{3+} ions. On the other hand, the O(4) ion is coordinated triangularly by three (6*h*) cations. Even if these are trivalent lanthanide ions, the sum of the electrostatic bond strength of the cations toward O(4), ζ, is only 9/7, considerably less than 2 as required by Pauling's electrostatic valence principle. This results in a very short Ln−O distance. Further calculation shows that ζ for the other oxygen ion does not differ significantly from 2. From this it follows that it must be very unfavorable to have cations with low charge in the (6*h*) sites in these compounds. Therefore, the Ca^{2+}/Mn^{2+} ions occupy CN = 9 (4*f*) sites. The effective ionic radii for seven-coordinated Y^{3+}, Ce^{3+}, and Tb^{3+} are 0.96, 1.07, 0.98 Å, respectively; whereas the effective ionic radii for Ca^{2+} and Mn^{2+} ions in 4*f* sites are 1.18 and 0.90 Å, respectively. In view of the similar ion radius and valence, the Mn^{2+} and Ce^{3+}/Tb^{3+} ions are expected to substitute of the Ca^{2+} and Y^{3+} sites in $Ca_4Y_6(SiO_4)_6O$ crystal structure, respectively. The structure parameters and ion radii for the given coordination number (CN) are listed in Table S1 in the Supporting Information.[33]

Photoluminescence Properties. Figure 2a−c shows the PLE and PL spectra of CYS: 10 mol % Ce^{3+} sample, respectively. Under 284 nm UV-light radiation, CYS: 10 mol % Ce^{3+} shows a blue emission (Figure 2b, black solid line) due to the $5d^1 \rightarrow 4f^1$ transition of Ce^{3+} consisting of a broad band from 350 to 600 nm with the maximum at 424 nm and a shoulder at 393 nm. It is well-known that the Ce^{3+} emission should be composed of a double band in view of the splitting of its ground state. The energy difference of this splitting between $^2F_{7/2}$ and $^2F_{5/2}$ of Ce^{3+} is about 2000 cm^{-1}.[19] Although the energy difference between 393 and 424 nm is about 1960 cm^{-1}, which is close to 2000 cm^{-1}. Therefore, the emission of Ce^{3+} at 393 and 424 nm should be contributed to the splitting of Ce^{3+} ground state. The corresponding excitation spectrum of CYS: 10 mol % Ce^{3+} sample includes two broad bands: a stronger

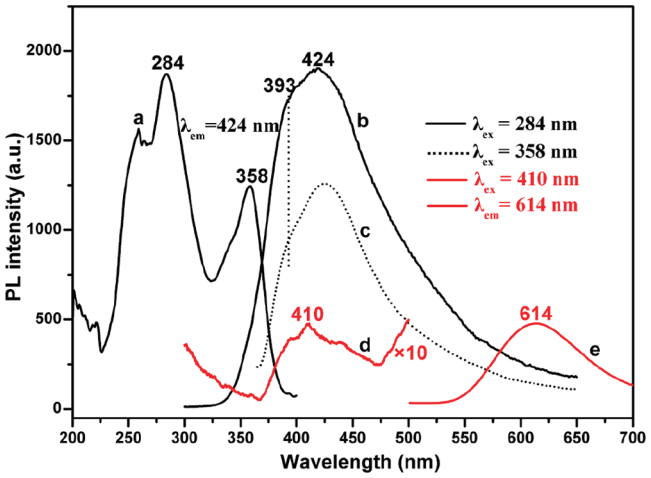

Figure 2. Typical (a, d) photoluminescence excitation (PLE) and (b/c, e) photoluminescence emission (PL) spectra of CYS: 10 mol % Ce^{3+} and CYS: 3 mol % Mn^{2+}, respectively. (d) The spectra overlap between the PL spectrum of CYS: 10 mol % Ce^{3+} and PLE spectrum of CYS: 3 mol % Mn^{2+}.

band from 225 to 320 nm centering at 284 nm and a weaker broad band from 320 to 380 nm centering at 358 nm with the maximum at 284 nm. The similar PL results are held for monitoring at 358 nm UV except for a lower intensity (Figure 2c, black dot line). This blue emission also can be validated by their CIE chromaticity coordinates such as (0.184, 0.155) for λ_{ex} = 284 nm and (0.184, 0.137) for λ_{ex} = 358 nm (see Table S2 in the Supporting Information). In addition, the quantum yields of CYS: 10 mol % Ce^{3+} were measured at 284 and 255 nm UV excitation to be 31% and 28%, respectively. This quantum yield difference is consistent with their PL intensity result. Figure S2 (Supporting Information) shows the PL intensity of Ce^{3+} as a function of its doping concentration (x, mol %) in CYS: x mol % Ce^{3+}. At first, the PL emission intensity of Ce^{3+} (λ_{ex} = 284, 358 nm) increases with the increase of its concentration (x), reaching a maximum value at 10, then decreasing with further increasing its concentration (x) due to the concentration quenching effect. Thus the optimum doping concentration for Ce^{3+} is 10 mol % of Y^{3+} in the CYS host. In general, the concentration quenching of luminescence is due to the energy migration among the activator ions at the high concentrations. In the energy migration process the excitation energy will be lost at a killer or quenching site, resulting in the decrease of luminescence intensity. The Mn^{2+} ions in solids generally show a broad band emission due to the $^4T_1 \rightarrow {}^6A_1$ transition within the $3d^5$ shell in which the electrons are strongly coupled to lattice vibration and affected by crystal field strength and site symmetry. The different crystal field strength on Mn^{2+} can tune the emission color point, which varies from green (strong crystal field) to orange/red (weak crystal field).[14,15] In view of the identical charge (+2) of Ca^{2+} and Mn^{2+} ions, the Mn^{2+} ion enters 4*f* sites by replacing Ca^{2+} in $Ca_4Y_6(SiO_4)_6O$. So Mn^{2+} shows orange-red emission in $Ca_4Y_6(SiO_4)_6O$ host based on its high coordination number (nine) and strong crystal field. Figure 2d and 2e shows the typical PLE and PL spectra of CYS: 3 mol % Mn^{2+} sample under UV excitation. For CYS: 3 mol % Mn^{2+}, the d−d transitions of Mn^{2+} are forbidden in view of spin and parity, so their excitation transitions are difficult to pump and emission intensity is very weak. The broad emission band centered at 614 nm is attributed to the spin-forbidden

$^4T_1(4G) \rightarrow {}^6A_1(6S)$ transition of Mn^{2+}. The corresponding excitation spectrum mainly consists of a broad band centering at 410 nm due to the transitions from $^6A_1(6S)$ to $^4A_1(^4G)$, $^4E(^4G)$. The comparison of the PL spectra for CYS: 10 mol % Ce^{3+} and the PLE spectrum for CYS: 3 mol % Mn^{2+} in Figure 2b–d reveals a great spectral overlap between the emission band of Ce^{3+} centered at 424 nm and the Mn^{2+} excitation transitions of $^6A_1(6S) \rightarrow {}^4A_1(^4G)$, $^4E(^4G)$. Accordingly, an efficient resonance-type energy transfer from Ce^{3+} to Mn^{2+} is expected. This type of energy transfer is common and has been reported by Chen's group in other Ce^{3+} and Mn^{2+}-coactivated phosphors such as $CaAl_2Si_2O_8$: Ce^{3+}/Mn^{2+},[34] $Ca_9Y(PO_4)_7$: Ce^{3+}/Mn^{2+}.[35]

Figures 3a, c and b, d shows the variation in PL spectra and emission intensity of Ce^{3+} and Mn^{2+} in the CYS: 10 mol % Ce^{3+}, y mol % Mn^{2+} systems with the increase of Mn^{2+}-doping concentrations from 0 to 5 mol % under 284 and 358 nm UV excitation, respectively. Although the concentration of Ce^{3+} was fixed, the emission intensity of Ce^{3+} decreased with increasing Mn^{2+} concentration. While the emission intensity of Mn^{2+} increases with the increase of its concentration. This result reveals an efficient energy transfer from Ce^{3+} to Mn^{2+} in CYS host. In order to further validate the energy transfer from Ce^{3+} to Mn^{2+}, we investigated the lifetimes of Ce^{3+}. As described by Blasse,[11] the decay behavior of Ce^{3+} can be expressed by

$$I = I_0 \exp(-t/\tau) \quad (1)$$

where I and I_0 are the luminescence intensities at time t and 0, and τ is the luminescence lifetime. For the CYS: 10 mol % Ce^{3+}, y mol % Mn^{2+} (y = 0, 0.5, 1, 2, 3, 5) samples, the lifetime of Ce^{3+} decreases with increasing Mn^{2+} concentration, which are 85.60, 69.12, 51.72, 39.86 28.31, 24.52 ns, respectively. The luminescence lifetime of Ce^{3+} decreases with increasing Mn^{2+} concentration because the energy absorbed by Ce^{3+} transferred to Mn^{2+}, which is strong evidence for the energy transfer from Ce^{3+} to Mn^{2+}, as reported by previous researchers.[36−38]

In addition, the energy transfer efficiency from Ce^{3+} to Mn^{2+} was investigated. Generally, the energy transfer efficiency from a sensitizer to activator can be expressed as the following equation[39−41]

$$\eta_T = 1 - \frac{I_S}{I_{S0}} \quad (2)$$

where η_T is the energy transfer efficiency and I_{S0} and I_S are the luminescence intensity of a sensitizer in the absence and presence of an activator, respectively. In the CYS: 10 mol % Ce^{3+}, y mol % Mn^{2+} systems, Ce^{3+} is the sensitizer and Mn^{2+} is the activator. Figure 4 shows the results of energy transfer efficiency from Ce^{3+} to Mn^{2+} calculated by eq 2 under different UV excitation. As shown in Figure 4, the energy transfer efficiency increases with increasing Mn^{2+} concentration under 284 nm UV radiation. However, the increscent rate of the emission intensity gradually decreases with the increase of Mn^{2+} concentration. The same trend in the energy transfer efficiency from Ce^{3+} to Mn^{2+} under 358 nm UV excitation is observed. This result reveals that the energy transfer from Ce^{3+} to Mn^{2+} will trend to saturation with a continuous increase of Mn^{2+} concentration due to the fixed Ce^{3+} concentration. The maximum energy transfer efficiency can reach 71% and 65% under 284 and 358 nm UV excitation, respectively. The results indicate that the energy transfer from Ce^{3+} to Mn^{2+} is very efficient. The different efficiency of a resonant energy transfer under different UV excitation should be attributed to different excitation energy absorption of Ce^{3+} f–d transitions. Because the excitation spectrum of CYS: Ce^{3+} shows two broad bands: a stronger band from 225 to 320 nm centering at 284 nm and a weaker broad band from 320 to 380 nm centering at 358 nm. The two bands are attributed to the transition of the Ce^{3+} ions from the 5d excited state to the $^2F_{5/2}$ and $^2F_{7/2}$ ground states. Obviously, the former excitation band has the larger excitation energy than the later excitation band. In other words, the CYS: Ce^{3+} sample has the larger energy absorption at 284 nm than at 358 nm UV radiation. Therefore, there are different energy transfer efficiencies when they transfer energy into Ce^{3+} ions under different UV radiation.

There are main two aspects to be responsible for the resonant energy-transfer mechanism: one is exchange interaction and the

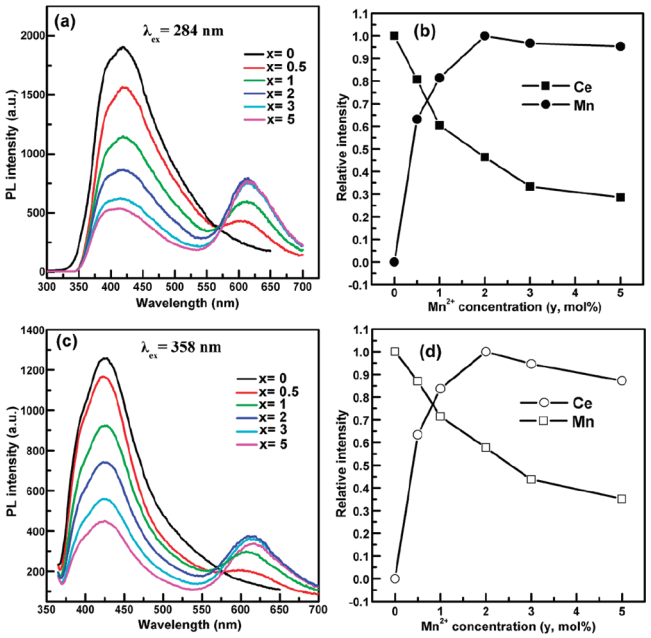

Figure 3. Dependence of (a, c) PL spectra and (b, d) emission intensity of Ce^{3+} and Mn^{2+} in the CYS: 10 mol % Ce^{3+}, y mol % Mn^{2+} samples on the Mn^{2+} concentrations (y = 0–5) monitoring with 284 and 358 nm UV, respectively.

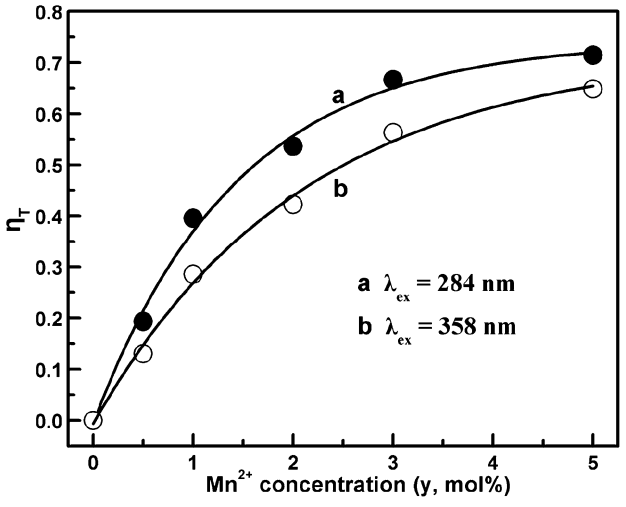

Figure 4. Energy transfer efficiency (η_T) from Ce^{3+} to Mn^{2+} in CYS: 10 mol % Ce^{3+}, y mol % Mn^{2+} (y = 0–5) samples under (a) 284 and (b) 358 nm UV excitation.

dx.doi.org/10.1021/am201335d | ACS Appl. Mater. Interfaces 2012, 4, 296–305

other is multipolar interaction.[42,43] It is known that if energy transfer results from the exchange interaction, the critical distance between the sensitizer and activator should be shorter than 4 Å.[43] In many cases, concentration quenching is due to energy transfer from one activator to another until an energy sink in the lattice is reached.[44] The critical distance R_C for energy transfer from the Ce^{3+} to Mn^{2+} ions can be calculated using the concentration quenching method. According to Blasse,[45] the distance between Ce^{3+} and Mn^{2+} ions can be expressed by

$$R_{Ce-Mn} = 2\left[\frac{3V}{4\pi X_{Ce-Mn} N}\right]^{1/3} \quad (3)$$

where N is the number of available sites for the dopant in the unit cell, X is the total concentration of Ce^{3+} and Mn^{2+}, and V is the volume of the unit cell. For $Ca_4Y_6(SiO_4)_6O$ host, N = 10 and V = 514.96 Å^3 . When X_{Ce-Mn} reaches the critical distance X_C, the R_{Ce-Mn} is equal to R_C. The critical concentration X_C, at which the luminescence intensity of Ce^{3+} is half of that in the sample in the absence of Mn^{2+}, is 0.16. Therefore, the critical distance (R_C) of energy transfer was calculated to be about 8.5 Å. It is observed that the radiative emission from Ce^{3+} prevails when $R_{Ce-Mn} > R_C$ and energy transfer from Ce^{3+} to Mn^{2+} dominates when $R_{Ce-Mn} < R_C$. This value is longer than 4 Å, indicating little possibility of energy transfer via the exchange interaction mechanism. Thus, the electric multipolar interaction can take place for energy transfer between the Ce^{3+} and Mn^{2+} ions. On the basis of Dexter's energy-transfer expressions of multipolar interaction and Reisfeld's approximation, the following relation can be given[42−45]

$$\frac{\eta_{S0}}{\eta_S} \propto C^{n/3} \quad (4)$$

where η_{S0} and η_S are the luminescence quantum efficiency of Ce^{3+} in the absence and presence of Mn^{2+}; C is the sum of the content of Ce^{3+} and Mn^{2+}; n = 6, 8, and 10 corresponding to dipole−dipole, dipole−quadrupole, and quadrupole−quadrupole interactions, respectively. The value η_{S0}/η_S is approximately calculated by the ratio of related luminescence intensities as[34,35]

$$\frac{I_{S0}}{I_S} \propto C^{n/3} \quad (5)$$

where I_{S0} is the intrinsic luminescence intensity of Ce^{3+}, and I_S is the luminescence intensity of Ce^{3+} in the presence of the Mn^{2+}. The $I_{S0}/I_S - C^{n/3}$ plots are shown in Figure 5, and the relationships are observed when n = 6, 8, and 10. A linear relationship was only observed when n = 8. This clearly indicates that the energy-transfer mechanism from the Ce^{3+} to Mn^{2+} ions is a dipole−quadrupole intereaction. Therefore, the electric dipole−quadrupole interaction predominates in the energy-transfer mechanism from the Ce^{3+} and Mn^{2+} ions in CYS host.

Considering the dipole−quadrupole interaction, the transfer probability is given by Dexter[44] as

$$P_{Ce-Mn}^{DQ} = 0.63 \times 10^{28} \frac{f_q \lambda_S^2 Q_A}{\tau_{S0} f_d R_{Ce-Mn}^8 E_S^4} \int F_S(E) F_A(E) dE \quad (6)$$

where $Q_A = 4.8 \times 10^{-16}$, f_d (1×10^{-7}) is the absorption cross-section of Mn^{2+}, and f_q (1×10^{-10}) are the oscillator strengths of dipole−quadrupole electrical absorption transitions for Mn^{2+}; λ_S (in Å) and E (in eV) are emission wavelength and emission energy of Ce^{3+}; $\int F_S(E)F_A(E)dE$ represents the spectral overlap between the normalized shapes of the Ce^{3+} emission $F_S(E)$ and Mn^{2+} excitation $F_A(E)$, and it is estimated at about 4.07 eV^{-1}. The critical distance (R_C) of energy transfer from Ce^{3+} to Mn^{2+} is defined as the distance for which the probability of transfer equals the probability of radiative emission of Ce^{3+}, i.e., the distance for which $P_{Ce-Mn}\tau_{S0} = 1$. Therefore, R_C can be found from eq 6[18,34,46]

$$R_C^8 = \frac{3.024 \times 10^{12} \lambda_S^2 f_q}{E_S^4} \int F_S(E) F_A(E) dE \quad (7)$$

In our case, the critical distance of energy transfer was calculated to be about 9.9 Å. This result is in good agreement with that obtained using the concentration quenching method, which further reveals that the mechanism of energy transfer from the Ce^{3+} to Mn^{2+} ions is mainly due to a dipole−quadrupole interaction.

Tb^{3+} has a relatively simple 4f-comfigurational energy level structure: low-energy state ^7F_j (j = 6, 5..., 0) and excited states $^5D_3$ and $^5D_4$. Generally, with a very low concentration of Tb^{3+} doped into host matrix, the transitions of $^5D_3$ to ^7F_j dominate and produce the blue emissions. As Tb^{3+} concentration increases, the cross relaxation from $^5D_3$ to $^5D_4$ occurs because of the Tb^{3+} ion interaction, which increases the population of the $^5D_4$ energy level, correspondingly enhancing the transitions of $^5D_4$ to ^7F_j, which emit a green light.[13,19,21] Figure 6a shows the PLE and PL spectra of CYS: 2 mol % Tb^{3+} sample. The excitation spectrum of CYS: 2 mol % Tb^{3+} shows a broad

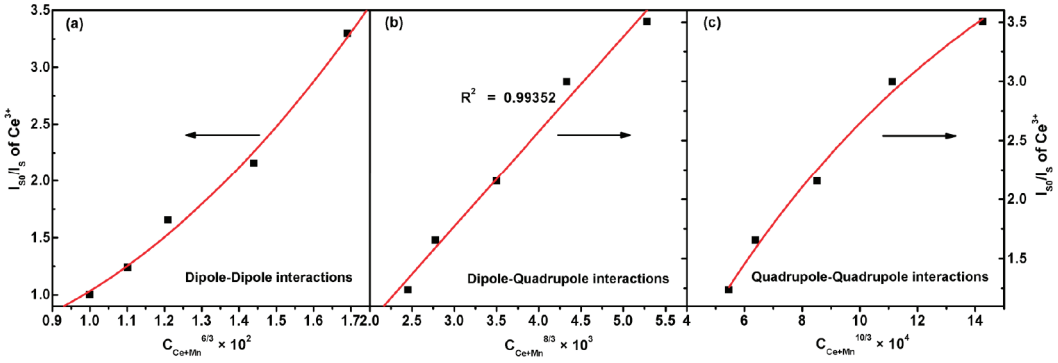

Figure 5. Dependence of I_{S0}/I_S of Ce^{3+} on (a) $C_{Ce+Mn}^{6/3} \times 10^2$, (b) $C_{Ce+Mn}^{8/3} \times 10^3$ and (c) $C_{Ce+Mn}^{10/3} \times 10^4$.

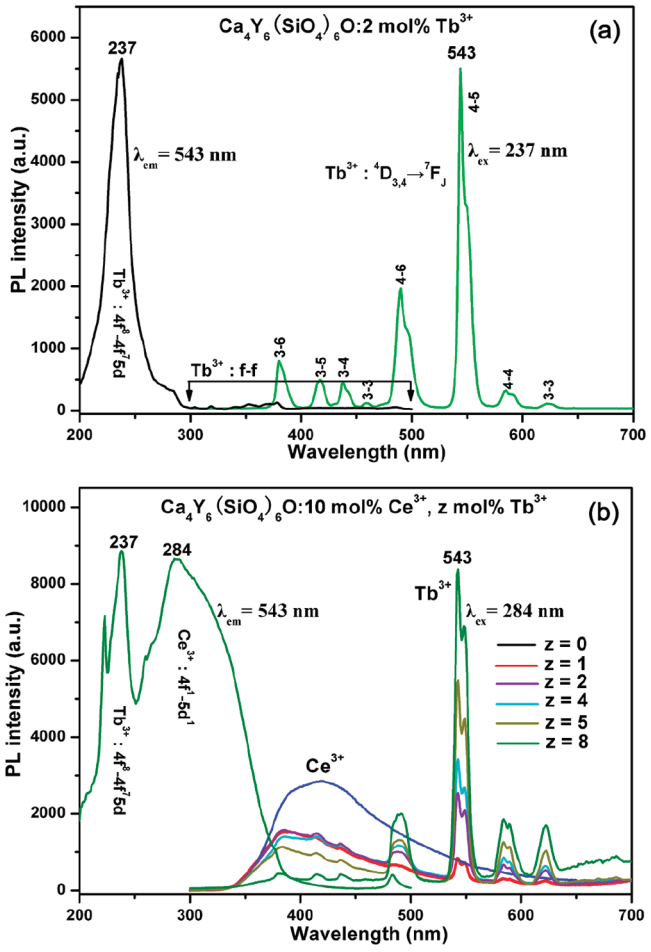

Figure 6. Typical PLE and PL spectra of (a) CYS: 2 mol % Tb^{3+} and (b) CYS: 10 mol % Ce^{3+}, z mol % Tb^{3+} (z = 0–8) samples.

band from 200 to 280 nm with a maximum at 237 nm and some weak transitions from 300 to 500 nm. The former is related to the $4f^8$–$4f^7$5d transition of Tb^{3+}, and the latter is due to its intra-(4f) transitions. Under 237 nm UV radiation excitation, the as-prepared CYS: 2 mol % Tb^{3+} gives green emission, and the obtained emission spectrum consists of the f-f transition lines within the Tb^{3+} $4f^8$ electron configuration, i.e., $^5D_3 \rightarrow {}^7F_6$ (380 nm), $^5D_3 \rightarrow {}^7F_5$ (417 nm), $^5D_3 \rightarrow {}^7F_4$ (438 nm), $^5D_3 \rightarrow {}^7F_3$ (458 nm), $^5D_4 \rightarrow {}^7F_6$ (490 nm), $^5D_4 \rightarrow {}^7F_5$ (543 nm), $^5D_4 \rightarrow {}^7F_4$ (584 nm), and $^5D_4 \rightarrow {}^7F_3$ (622 nm), respectively. The Ce^{3+} ion is a well-known sensitizer for trivalent rare earth ion luminescence, and the sensitizing effects depend strongly on the host lattices into which these ions are introduced.[19−21] The Tb^{3+} emission in $Ca_4Y_6(SiO_4)_6O$ can be sensitized by Ce^{3+}, which is due to the fact that the emission band of Ce^{3+} in the range 350–550 nm overlaps with the f–f excitation peaks of Tb^{3+} at 350–500 nm, as shown in the Figure 6a and 6b. A typical excitation and emission spectrum for a sample with composition CYS: 10 mol % Ce^{3+}, 5 mol % Tb^{3+} is shown in Figure 6b. The excitation spectrum monitoring with $Tb^{3+}{}^5D_4 \rightarrow {}^7F_5$ emission (543 nm) clearly shows two bands: 200–250 nm centered at 237 nm and 250–380 nm with the maximum at 284 nm. The first band is due to absorption of Tb^{3+} $4f^8$–$4f^7$5d transition and the latter is caused by Ce^{3+} 4f–-$5d^1$ transition. The presence of the Ce^{3+} excitation band suggests energy transfer from Ce^{3+} to Tb^{3+}. In addition, upon excitation into the Ce^{3+} absorption band, the emission spectrum of CYS: 10 mol % Ce^{3+}, z mol % Tb^{3+} (z = 0–8) samples (Figure 6b) not only shows both Ce^{3+} and Tb^{3+} emission but also the emission intensity of Ce^{3+} decreases with the increase of Tb^{3+} concentration (z, mol %), which further confirm the existence of energy transfer from Ce^{3+} to Tb^{3+}. In view of the $Ce^{3+} \rightarrow Tb^{3+}$ energy transfer in CYS, the emission colors of CYS: 10 mol % Ce^{3+}, z mol % Tb^{3+} (z = 0–8) phosphors can be tuned from blue to green by changing the doping concentration of Tb^{3+} ion. The quantum yields (25%-38%) and CIE color coordinates of CYS: 10 mol % Ce^{3+}, z mol % Tb^{3+} (z = 0–8) phosphors under 284 nm UV excitation are listed in Table S2 in the Supporting Information.

As we know, energy transfer from sensitizer to activator is a feasible route to realize color-tunable emission, and a white light emission can be obtained through mixing the tricolor (RGB) light sources at a suitable ratio.[9] In our case, the CYS: Ce^{3+} emits bright blue light due to the 5d–4f transition of Ce^{3+}, and the efficient energy transfer of $Ce^{3+} \rightarrow Mn^{2+}$ is also validated in Ce^{3+}/Mn^{2+}-coactivated CYS phosphors. Thus, it is reasonable to predict that the color-tunable emissions from blue light to orange-red light in CYS: Ce^{3+}, Mn^{2+} systems can be obtained. In addition, a color-tunable emission from blue to green can also be realized in CYS: Ce^{3+}, Tb^{3+} samples through the $Ce^{3+} \rightarrow Tb^{3+}$ energy transfer. Thus, it is possible to produce white emission due to the simultaneous appearance of RGB light by appropriately adjusting of the doping concentration of Mn^{2+} and Tb^{3+} at a fixing the Ce^{3+} (sensitizer) concentration in the present CYS host. Our experiments have confirmed the above situation. A series of CYS: 10 mol % Ce^{3+}, y mol % Mn^{2+}, z mol % Tb^{3+} samples with different Mn^{2+} and Tb^{3+} concentrations (y = 0–6, z = 0–8) have been synthesized. Figure 7 shows the typical PL spectra of CYS: 10 mol % Ce^{3+}, y mol % Mn^{2+}, z mol % Tb^{3+} samples (y = 2, 3, 4; z = 1, 2, 4) under different wavelengths UV excitation (a: 284 nm; b: 358 nm), respectively. The quantum yields (QYs) and CIE color coordinates (X, Y) of the CYS: Ce^{3+}, Mn^{2+}, Tb^{3+} samples under UV excitation (λ_{ex} = 284 and 358 nm) are summarized in Table S2 in the Supporting Information. As shown in Figure 4a, the emission spectra of CYS: 10 mol % Ce^{3+}, y mol % Mn^{2+} samples are composed of blue emission of Ce^{3+} and orange-red emission of Mn^{2+} ($^4T_1 \rightarrow {}^6A_1$), and the blue emission gradually decrease and orange-red emission gradually increase with the increase of Mn^{2+} concentration. Therefore, the emitting colors of CYS: Ce^{3+}, Mn^{2+} samples are gradually tuned from blue to orange-red by changing the Mn^{2+} concentrations. The quantum yields of CYS: 10 mol % Ce^{3+}, y mol % Mn^{2+} (y = 1–6) samples are measured to be 13–26% for λ_{ex} = 284 nm and 13–24% for λ_{ex} = 358 nm, respectively. On the other hand, when codoping Ce^{3+} and Tb^{3+} into CYS host, the PL spectra of CYS: 10 mol % Ce^{3+}, z mol % Tb^{3+} samples consists of 5d–4f transition of Ce^{3+} and $^5D_4 \rightarrow {}^7F_J$ (J = 6–2) transitions of Tb^{3+} (Figure 6b), and the emitting colors of CYS: 10 mol % Ce^{3+}, z mol % Tb^{3+} samples are tuned from blue to green through changing Tb^{3+} concentration with a quantum yield range from 25% to 38%. The above results are also confirmed by their CIE color coordinates shown in Table S2 in the Supporting Information and Figure 8. From Figure 8, it is clearly seen that the CIE coordinates of CYS: 10 mol % Ce^{3+}, y mol % Mn^{2+} (y = 0–6) and CYS: 10 mol % Ce^{3+}, z mol % Tb^{3+} (z = 0–8) samples under 284 nm UV excitation move from blue region to orange-red region (arrow line a) and from blue region to green region (arrow line b) with the increase of y and z values, respectively. More importantly, wide-range-tunable white emissions have be obtained by precisely control the contents of Mn^{2+} and Tb^{3+} ions, as shown in the spectra of Figure 7 and the points 1–8 in Figure 8. When fixed the y at 3, the CIE coordinate

dx.doi.org/10.1021/am201335d | ACS Appl. Mater. Interfaces 2012, 4, 296–305

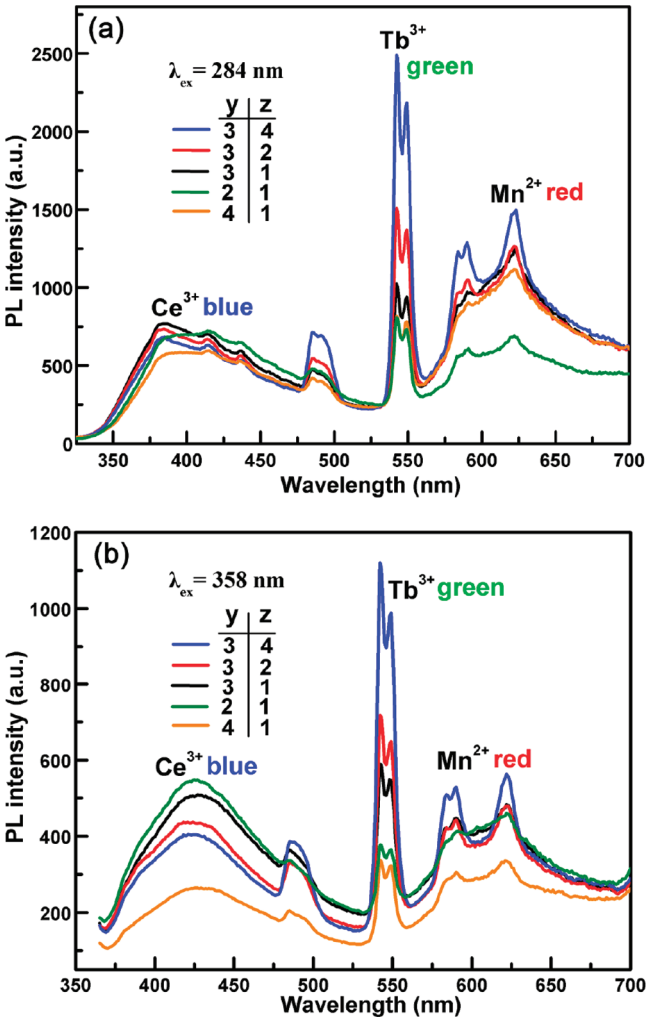

Figure 7. PL spectra of CYS: 10 mol % Ce^{3+}, *y*mol % Mn^{2+}, *z* mol % Tb^{3+} samples (*y* = 2, 3, 4; *z* = 1, 2, 4) under different wavelengths UV excitation: (a) 284 nm and (b) 358 nm.

position of CYS: 10 mol % Ce^{3+}, 3 mol % Mn^{2+}, *z* mol % Tb^{3+} moves from point 1 to 2 and then to 3 with the increase of *z* values from 1 to 2, and to 4, namely, the increase of green component. While fixed the *z* at 1, the CIE coordinate position of CYS: 10 mol % Ce^{3+}, 3 mol % Mn^{2+}, *z* mol % Tb^{3+} moves from point 4 to 1, and to 5 with the increase of y values from 2 to 3, and to 4, namely, the increase of red component. The single-composition trichromatic white emission by tridoping the Ce^{3+}, Mn^{2+}, Tb^{3+} ions has been previously reported in $Ca_3Y(GaO)_3(BO_3)_4$ system by Chen's group.[9] However, the trichromatic emissions of Ce^{3+}, Mn^{2+}, Tb^{3+} ions in $Ca_3Y(GaO)_3(BO_3)_4$ system are attributed to the $Ce^{3+}\rightarrow Mn^{2+}$ ET and the coexcitation of Ce^{3+} and Tb^{3+}, which is different from the dual ETs of $Ce^{3+}\rightarrow Mn^{2+}$ and $Ce^{3+}\rightarrow Tb^{3+}$ in current CYS system. Moreover, the warmer white-light emissions by tridoping the Ce^{3+}, Mn^{2+}, and Tb^{3+} ions have be obtained in CYS system than in $Ca_3Y(GaO)_3(BO_3)_4$ system through the comparison of CIE color coordinates in Table 1 and the date in ref 9. In addition, the similar results are held for the CYS: 10 mol % Ce^{3+}, 3 mol % Mn^{2+}, *z* mol % Tb^{3+} samples under 358 nm UV excitation, as shown in Table S2 in the Supporting Information. In our study, we also found that the relative intensity of RGB emission can be tuned by the variation of excitation UV light. When changing the UV excitation

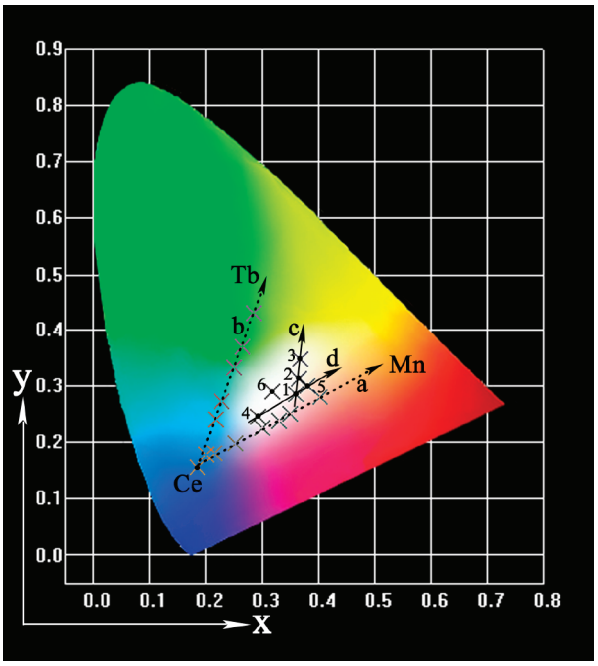

Figure 8. CIE chromaticity diagram for CYS: 10 mol % Ce^{3+}, *y* mol % Mn^{2+}, *z* mol % Tb^{3+} samples under 284 nm UV excitation: (1) *y* = 3, *z* = 1; (2) *y* = 3, *z* = 2; (3) *y* = 3, *z* = 4; (4) *y* = 2, *z* = 1; (5) *y* = 4, *z* = 1; and under 358 nm UV excitation: (6) *y* = 3, *z* = 1, and *c* and *d* represent CIE color coordinate variation with the Tb^{3+} and Mn^{2+} concentrations, respectively. *a* and *b* represents the variation of CIE color coordinates of CYS: 10 mol % Ce^{3+}, *y* mol % Mn^{2+} (*y* = 0−6) and CYS: 10 mol % Ce^{3+}, *z* mol % Tb^{3+} (*z* = 0−8) samples with the *y* and *z* values, respectively.

Table 1. CIE Color Coordinates (*X*, *Y*) of the CYS: *x* mol % Ce^{3+}, *y* mol % Mn^{2+}, *z* mol % Tb^{3+} (y = 0.5-8; *z* = 1−8) under Low Voltage Electron Beam (accelerating voltage = 3.0 kV; filament current = 90 mA)

sample	chromaticity color coordinate (*X*, *Y*)
CYS: 10 mol % Ce^{3+}	(0.164, 0.137)
CYS: 10 mol % Ce^{3+}, 0.5 mol % Mn^{2+}	(0.203, 0.161)
CYS: 10 mol % Ce^{3+}, 1 mol % Mn^{2+}	(0.223, 0.172)
CYS: 10 mol % Ce^{3+}, 2 mol % Mn^{2+}	(0.259, 0.183)
CYS: 10 mol % Ce^{3+}, 3 mol % Mn^{2+}	(0.322, 0.214)
CYS: 10 mol % Ce^{3+}, 5 mol % Mn^{2+}	(0.365, 0.232)
CYS: 10 mol % Ce^{3+}, 8 mol % Mn^{2+}	(0.411, 0.268)
CYS: 10 mol % Ce^{3+}, 1 mol % Tb^{3+}	(0.203, 0.242)
CYS: 10 mol % Ce^{3+}, 2 mol % Tb^{3+}	(0.227, 0.348)
CYS: 10 mol % Ce^{3+}, 4 mol % Tb^{3+}	(0.243, 0.401)
CYS: 10 mol % Ce^{3+}, 5 mol % Tb^{3+}	(0.256, 0.461)
CYS: 10 mol % Ce^{3+}, 8 mol % Tb^{3+}	(0.271, 0.466)
CYS: 10 mol % Ce^{3+}, 3 mol % Mn^{2+}, 1 mol % Tb^{3+}	(0.326, 0.308)
CYS: 10 mol % Ce^{3+}, 3 mol % Mn^{2+}, 2 mol % Tb^{3+}	(0.328, 0.331)
CYS: 10 mol % Ce^{3+}, 3 mol % Mn^{2+}, 4 mol % Tb^{3+}	(0.331, 0.354)
CYS: 10 mol % Ce^{3+}, 4 mol % Mn^{2+}, 2 mol % Tb^{3+}	(0.365, 0.313)
CYS: 10 mol % Ce^{3+}, 5 mol % Mn^{2+}, 2 mol % Tb^{3+}	(0.357, 0.295)

wavelength from 292 to 358 nm, the relative PL intensity of green and red to blue emission of representative CYS: 10 mol % Ce^{3+}, 3 mol % Mn^{2+}, 1 mol % Tb^{3+} sample changes, which results in its CIE coordinate position moves from point 1 (0.336, 0.286) to point 6 (0.318, 0.289) shown in Figure 8. Generally, a wide-range-tunable white light emission from cool to warm white

dx.doi.org/10.1021/am201335d | ACS Appl. Mater. Interfaces 2012, 4, 296−305

emission with high quantum yields (13−30%) were obtained in CYS: Ce^{3+}, Mn^{2+}, Tb^{3+} samples by the dual energy transfer of $Ce^{3+} \rightarrow Mn^{2+}$ and $Ce^{3+} \rightarrow Tb^{3+}$ as well as the use of different UV sources. Hence, this material would be potentially used as a single phase white-light-emitting source in UV-LEDs (284, 358 nm).

Cathodoluminescence Properties. In order to explore the potential of the as-synthesized CYS: $Ce^{3+}/Mn^{2+}/Tb^{3+}$ samples to be used as CL materials, their CL properties have been investigated in detail. Figure 9 shows the CL spectra of

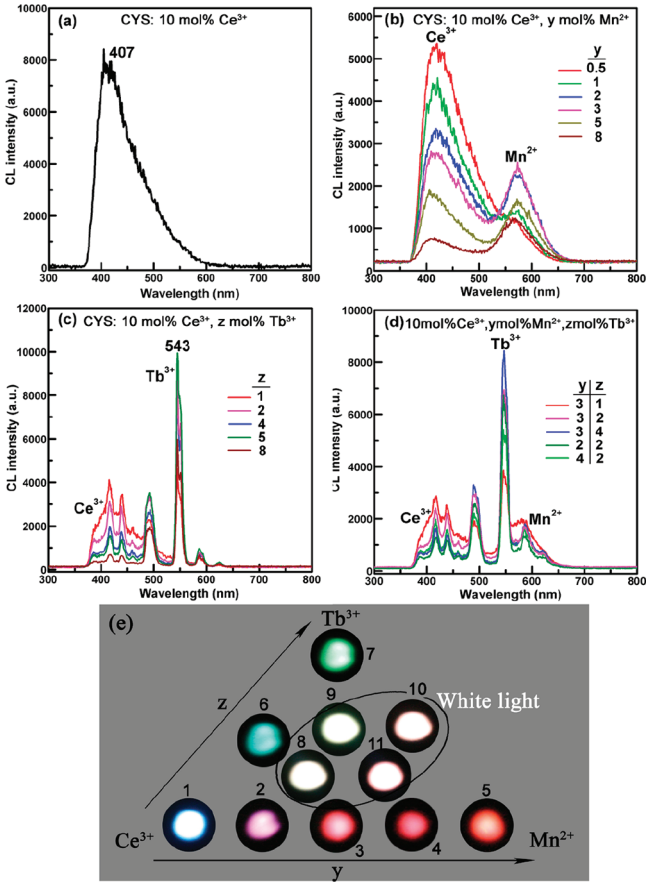

Figure 9. CL spectra of (a) CYS: 10 mol % Ce^{3+}; (b) CYS: 10 mol % Ce^{3+}, *y* mol % Mn^{2+}; (c) CYS: 10 mol % Ce^{3+}, *z* mol % Tb^{3+}; and (d) CYS: 10 mol % Ce^{3+}, *y* mol % Mn^{2+}, *z* mol % Tb^{3+} samples at different Mn^{2+} and Tb^{3+} concentrations, $y = 0-18$; $z = 0-8$. (e) Luminescent photographs of CYS: 10 mol % Ce^{3+}, *y* mol % Mn^{2+}, *z* mol % Tb^{3+} samples: (1) $y = 0$, $z = 0$, (2) $y = 1$, $z = 0$, (3) $y = 3$, $z = 0$, (4) $y = 5$, $z = 0$, (5) $y = 8$, $z = 0$, (6) $y = 0$, $z = 2$, (7) $y = 0$, $z = 8$, (8) $y = 3$, $z = 1$, (9) $y = 3$, $z = 2$, (10) $y = 4$, $z = 2$, (11) $y = 5$, $z = 2$. (Accelerating voltage = 3.0 kV, Filament current = 90 mA).

CYS: 10 mol % Ce^{3+}, *y* mol % Mn^{2+}, *z* mol % Tb^{3+} ($y = 0-18$; $z = 0-8$) samples at different Ce^{3+}, Mn^{2+}, and Tb^{3+} concentrations, whose profiles are similar to their PL spectra. The insets 1−11 in Figure 9e shows its corresponding digital luminescence photographs. The CIE chromaticity coordinates of the studied samples under accelerating voltage = 3.0 kV and filament current = 90 mA electron beam radiation are listed in Table 1. Under the low-voltage electron beam excitation, pure CYS: 10 mol % Ce^{3+} sample gives bright blue emission (Figure 9e, inset 1), whose emission spectrum consists of a broad band (370−500 nm) centered at 407 nm due to the $5d^1 \rightarrow 4f^1$ transition of Ce^{3+}. The blue emission of CYS: 10 mol % Ce^{3+} can be determined by its CIE coordinate (0.164, 0.137) calculated through its CL spectrum. The CL emission spectrum of CYS: 10 mol % Ce^{3+} has a slight difference than that of PL spectrum, which could result from different excitation source. When codoping Ce^{3+} and Mn^{2+} into the CYS host, maintaining the Ce^{3+} concentration at 10 mol % and changing the Mn^{2+} concentration from 0.5 to 6 mol %, the CL intensity of Ce^{3+} gradually decreases and the CL intensity of Mn^{2+} gradually increases with the increase of Mn^{2+} concentration, as shown in Figure 9b. The results reveal that an efficient energy transfer occurs from Ce^{3+} to Mn^{2+} ions in the CYS host and the CL colors of CYS: Ce^{3+}, Mn^{2+} could be gradually transformed from blue to orange-red (Figure 9e, insets 1−5). For the CYS: Ce^{3+}, Tb^{3+} samples such as CYS: 10 mol % Ce^{3+}, *z* mol % Tb^{3+} ($z = 1-8$), their CL spectra (Figure 9c) consist of the characteristic transitions of Ce^{3+} and Tb^{3+}, and their CL colors can be changed from blue to green due to $Ce^{3+} \rightarrow Tb^{3+}$ energy transfer, as shown in Table 1. Because CYS: Ce^{3+}, Tb^{3+} can give a blue-green emission at a proper Tb^{3+} doping concentration due to the $Ce^{3+} \rightarrow Tb^{3+}$ energy transfer and CYS: Ce^{3+}, Mn^{2+} shows an orange-red emission due to the $Ce^{3+} \rightarrow Mn^{2+}$ energy transfer under low-voltage electron beam excitation, it is possible to obtain white light emission in the CYS host lattice by codoping with Ce^{3+}, Tb^{3+}, and Mn^{2+} and appropriately adjusting their concentrations. In our experiment, we have obtained excellent white light emission in the CYS: Ce^{3+}, Mn^{2+}, Tb^{3+} systems. Figure 9d shows the CL spectrum of the CYS: 10 mol % Ce^{3+}, *y* mol % Mn^{2+}, *z* mol % Tb^{3+} ($y = 2, 3, 4$; $z = 1, 2, 4$) samples. Under low-voltage electron beam excitation, the CYS: 10 mol % Ce^{3+}, *y* mol % Mn^{2+}, *z* mol % Tb^{3+} samples simultaneously show the characteristic emission of sensitizer ion (Ce^{3+}, $5d^1 \rightarrow 4f^1$) and activator ions (Mn^{2+}, $4T^1 \rightarrow 6S^1$; Tb^{3+}, $^5D_{3,4} \rightarrow {}^7F_J$ ($J = 6-2$)). These emission lines of Ce^{3+}, Tb^{3+}, and Mn^{2+} cover the whole visible light region with tunable intensity, resulting in a tunable white light emission. The emissive color is bright white to the naked eye, as seen clearly from the luminescence photograph in the insets 8−11 of Figure 9e. The white emission can be further confirmed by their CIE coordinates, for example, (0.326, 0.308) for CYS: 10 mol % Ce^{3+}, 3 mol % Mn^{2+}, 1 mol % Tb^{3+}, (0.328, 0.331) for CYS: 10 mol % Ce^{3+}, 3 mol % Mn^{2+}, 2 mol % Tb^{3+}, (0.365, 0.313) for CYS: 10 mol % Ce^{3+}, 4 mol % Mn^{2+}, 2 mol % Tb^{3+} and (0.357, 0.295) for CYS: 10 mol % Ce^{3+}, 5 mol % Mn^{2+},*z* mol % Tb^{3+}, respectively. These as-prepared CYS: Ce^{3+}, Mn^{2+}, Tb^{3+} phosphors with tunable white emission have potential as back light source to apply in FEDs.

The CL emission intensities of representative white-light-emitting CYS: 10 mol % Ce^{3+}, 3 mol % Mn^{2+}, 2 mol % Tb^{3+} sample has been investigated as a function of the accelerating voltage and the filament current, as shown in Figure 10. When the filament current is fixed at 92 mA, the CL intensity increases with raising the accelerating voltage from 1.0 to 5.0 kV (Figure 10a). Similarly, under a 5.0 kV electron beam excitation, the CL intensity also increases with increasing the filament current from 82 to 94 mA (Figure 10b). There is no obvious saturation effect for the CL intensity of these samples with the increase of current density and accelerating voltage. The increase in CL brightness with an increase in electron energy and filament current is attributed to the deeper penetration of the electrons into the phosphor body and the larger electron-beam current density. The electron penetration depth can be

dx.doi.org/10.1021/am201335d | ACS Appl. Mater. Interfaces 2012, 4, 296−305

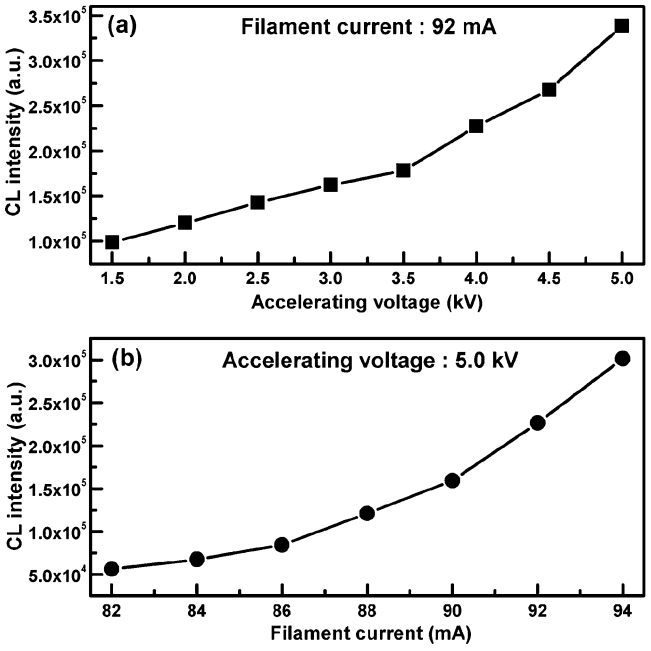

Figure 10. CL intensity of representative white-light-emitting CYS: 10 mol % Ce^{3+}, 3 mol % Mn^{2+}, 2 mol % Tb^{3+} sample as a function of (a) accelerating voltage and (b) filament current.

estimated using the empirical formula

$$L\ (\text{Å}) = 250\left(\frac{A}{\rho}\right)\left(\frac{E}{\sqrt{Z}}\right)^{n},\quad n = \frac{1.2}{1 - 0.29lgZ} \tag{8}$$

where A is the atomic or molecular weight of the material, ρ is the bulk density, Z is the atomic number or the number of electrons per molecule in the compounds, and E is the accelerating voltage (kV).[47,48] For example, for CYS: 10 mol % Ce^{3+}, 3 mol % Mn^{2+}, 2 mol % Tb^{3+}, $Z = 598$, $A = 1494$, $\rho = 3.94$ g/cm^3, the estimated electron penetration depth at 3.0 kV is about 27.5 nm. For CL of the above samples, the Ce^{3+}, Mn^{2+} and Tb^{3+} ions are excited by the plasma produced by the incident electrons. The deeper the electron penetration depth, the more plasma will be produced, which results in more activator ions being excited, and thus the CL intensity increases.

The degradation property for phosphor is very important for FED application. Thus we also investigated the degradation behavior of CYS: 10 mol % Ce^{3+}, 3 mol % Mn^{2+}, 2 mol % Tb^{3+} sample under low voltage electron beam excitation. Figure S3 in the Supporting Information (red line) shows the decay behavior of the CL intensity of representative CYS: 10 mol % Ce^{3+}, 3 mol % Mn^{2+}, 2 mol % Tb^{3+} sample under continuous electron beam bombardment when the accelerating voltage = 3.0 kV, filament current = 90 mA. The CL peaks are almost the same as those before electron bombardment. However, the CL intensity of the studied sample monotonously decreases with prolonging the electron bombardment time. After the continuous electron radiation for 1 h, the CL intensities of the studied sample fall to 88% of the initial value, respectively. This degradation of CL intensity may be due to the accumulation of carbon at the surface during electron bombardment.[49−51] Because the accretion of graphitic carbon during electron-beam exposure at high current densities is a well-known effect. This carbon contamination will prevent low-energy electrons from reaching the phosphor grains and also exacerbate surface charging, and thus lower the CL intensity. In addition, after stopping bombardment for a while, the CL intensity could not restore to the initial value, indicating permanent damage to the phosphor occurs, which is another reason to result in the decrease of the CL intensity. On the other hand, the Commission International del'Eclairge (CIE) chromaticity coordinates of the MYS-1Ce, 3Mn, 1Tb sample under a continuous electron beam radiation are measured to investigate the color stability and presented in Figure S3 in the Supporting Information (green line for x and blue line for y). Obviously, the CIE coordinate values are nearly invariable under a continuous electron radiation for 1 h, keeping x and y at about 0.328 and 0.331, respectively. In summary, the short time experiment (1 h) indicates that the stability of the CL intensity and CIE color coordinates stability of the as-prepared CYS: Ce^{3+}, Mn^{2+}, Tb^{3+} samples is good, which shows potential advantages in the FEDs.

4. CONCLUSION

In conclusion, Ce^{3+}, Mn^{2+}, Tb^{3+}-triactivated $Ca_4Y_6(SiO_4)_6O$ (CYS) oxyapatite structured phosphors have been prepared via solid state reaction. Under UV excitation, there exist dual energy transfer (ET), i.e., $Ce^{3+}\rightarrow Mn^{2+}$ and $Ce^{3+}\rightarrow Tb^{3+}$ in the CYS: Ce^{3+}, Mn^{2+}, Tb^{3+} systems. The energy transfer from Ce^{3+} to Mn^{2+} in CYS: Ce^{3+}, Mn^{2+} phosphors has been demonstrated to be a resonant type via a dipole−quadrupole mechanism, and the critical distance (R_C) calculated by quenching concentration method and spectral overlap method are 8.5 and 9.9 Å, respectively. By the dual ET of $Ce^{3+}\rightarrow Mn^{2+}$ and $Ce^{3+}\rightarrow Tb^{3+}$, the emitting colors of studied samples can be adjusted from blue to orange-red and from blue to green, respectively. More importantly, a wide-range-tunable white light emission with high quantum yields (13−30%) were obtained in CYS: Ce^{3+}, Mn^{2+}, Tb^{3+} samples by precisely controlling the contents of Ce^{3+}, Mn^{2+} and Tb^{3+} ions. Under low-voltage electron beam excitation, the CL spectra of the CYS: Ce^{3+}, Mn^{2+}, Tb^{3+} samples cover the whole visible light region, resulting in an excellent white light emission. After the continuous electron radiation for 1 h, the CL intensity of the white-emitting CYS: Ce^{3+}, Mn^{2+}, Tb^{3+} sample remains 89% of the initial value and its CIE coordinate are nearly invariable. The results indicate that the as-prepared CYS: Ce^{3+}, Mn^{2+}, Tb^{3+} phosphors have a good CL intensity and CIE coordinate stability under electron beam bombardment. Generally, the multicolor luminescence, and the white light with high quantuam yields and varied hues have been obtained in Ce^{3+}, Mn^{2+}, Tb^{3+}-activated CYS phosphors by utilizing the principle of energy transfer and properly designed activator contents under UV and electron beam excitation, which have potential as single-phase trichromatic white-emitting phosphors.

■ ASSOCIATED CONTENT

Supporting Information

Crystal structure of $Ca_4Y_6(SiO_4)_6O$ (Figure S1), structure parameters and ionic radii for given coordination number (Table S1), the PL intensity of CYS: Ce^{3+} samples as a function of Ce^{3+} concentration (Figure S2), quantum yields and chromaticity coordinates of the CYS: $Ce^{3+}/Mn^{2+}/Tb^{3+}$ samples under UV excitation (Table S2), dependence of relative CL intensity and CIE color coordinates of CYS: Ce^{3+}, Mn^{2+}, Tb^{3+} sample on the electron radiation time (Figure S3). This material is available free of charge via the Internet at http://pubs.acs.org/.

AUTHOR INFORMATION

Corresponding Author
*E-mail: jlin@ciac.jl.cn.

ACKNOWLEDGMENTS

This project is financially supported by National Basic Research Program of China (2010CB327704), and the National Natural Science Foundation of China (Grants NSFC 60977013 and 20921002).

REFERENCES

(1) Xie, R. J.; Hirosaki, N. *Sci. Technol. Adv. Mater.* **2007**, *8*, 588.
(2) Chen, D. Q.; Wang, Y. S.; Zheng, K. L.; Guo, T. L.; Yu, Y. L.; Huang, P. *Appl. Phys. Lett.* **2007**, *91*, 251903.
(3) Wang, J. W.; Tanner, P. A. *J. Am. Chem. Soc.* **2010**, *132*, 947.
(4) Babu, P.; Jang, K. H.; Rao, C. S.; Shi, L.; Jayasankar, C. K.; Lavín, V.; Seo, H. J. *Opt. Exp.* **2011**, *19*, 1836.
(5) Evans, R. C.; Carlos, L. D.; Douglas, P.; Rocha, J. *J. Mater. Chem.* **2008**, *18*, 1110.
(6) DiMaio, J. R.; Kokuoz, B.; Ballato, J. *Opt. Exp.* **2006**, *14*, 11412.
(7) Chen, G. Y.; Liu, Y.; Zhang, Y. G.; Somesfalean, G.; Zhang, Z. G.; Sun, Q.; Wang, F. P. *Appl. Phys. Lett.* **2007**, *91*, 133103.
(8) Yang, J.; Zhang, C. M.; Peng., C.; Li, C. X.; Wang, L. L.; Chai, R. T.; Lin, J. *Chem.—Eur. J.* **2009**, *15*, 4649.
(9) Huang, C. H.; Chen, T. M. *J. Phys. Chem. C* **2011**, *115*, 2349.
(10) Li, G. G.; Hou, Z. Y.; Peng, C.; Wang, W. W.; Cheng, Z. Y.; Li, C. X.; Lian, H. Z.; Lin, J. *Adv. Funct. Mater.* **2010**, *20*, 3446.
(11) Blasse, G.; Grabmarier, B. C.; *Luminescent Materials*; Sprinnger-Verlag: Berlin, Germany, 1994, *p96*, 18.
(12) Yang, S. H.; Lial, Y. J.; Cheng, N. J.; Ling, Y. H. *J. Alloys Compd.* **2010**, *489*, 689.
(13) Park, W. B.; Singh, S. P.; Pyo, M.; Sohn, K. S. *J. Mater. Chem.* **2011**, *21*, 5780.
(14) Blasse, G.; Grabmaier, B. C. *Luminescent Materials*; Springer-Verlag: Berlin, 1994, P52.
(15) Shi, L.; Huang, Y. L.; Seo, H. J. *J. Phys. Chem. A* **2010**, *114*, 6927.
(16) McKeever, S. W. S.; Brown, M. D.; Abbundi, R. J.; Chan, H.; Mathur, V. K. *J. Appl. Phys.* **1986**, *60*, 2505.
(17) Zhang, C. M.; Huang, S. S.; Yang, D. M.; Kang, X. J.; Shang, M. M.; Peng, C.; Lin, J. *J. Mater. Chem.* **2010**, *20*, 6674.
(18) Guo, N.; Huang, Y. J.; You, H. P.; Yang, M.; Song, Y. H.; Liu, K.; Zheng, Y. H. *Inorg. Chem.* **2010**, *49*, 10907.
(19) Lin, J.; Su, Q. *J. Mater. Chem.* **1995**, *5*, 1151.
(20) Chung, H. Y.; Lu, C. H.; Hsu, C. H. *J. Am. Ceram. Soc.* **2010**, *93*, 1838.
(21) Hsu, C. H.; Lu, C. H. *J. Mater. Chem.* **2011**, *21*, 2932.
(22) Psuja, P.; Hreniak, D.; Strek, W. *J. Nanomater.* **2007**, *2007*, 81350.
(23) Wang, Z. L.; Chan, H. L. W.; Li., H. L.; Hao, J. H. *Appl. Phys. Lett.* **2008**, *93*, 141106.
(24) Mao, Y. B.; Tran, T.; Guo, X.; Huang, J. Y.; Shih, C. K.; Wang., K. L.; Chang, J. P. *Adv. Funct. Mater.* **2009**, *19*, 748.
(25) Zhang, Q. H.; Wang, J.; Yeh, C. W.; Ke, W. C.; Liu, R. S.; Tang, J. K.; Xie, M. B.; Liang, H. B.; Su, Q. *Acta Mater.* **2010**, *58*, 6728.
(26) Lin, J.; Su, Q. *J. Mater. Chem.* **1995**, *5*, 603.
(27) Peng, C.; Li, G. G.; Kang, X. J.; Li, C. X.; Lin, J. *J. Colloid Interface Sci.* **2011**, *355*, 89.
(28) Lammers, M. J.; Blasse, G. *J. Electrochem. Soc.* **1987**, *134*, 2068.
(29) van Vliet, J. P. M; Blasse, G. *Mater. Res. Bull.* **1990**, *25*, 391.
(30) Shen, Y. Q.; Chen, R.; Xiao, F.; Sun, H. D.; Tok, A.; Dong, Z. L. *J. Solid. State. Chem.* **2010**, *183*, 3093.
(31) Blasse, G.; Bril, A. *J. Chem. Phys.* **1967**, *47*, 5139.
(32) Lammers, M. J. J.; Blasse., G. *J. Electrochem. Soc.* **1987**, *134*, 2068.
(33) Shannon, D. R. *Acta Crystallogr., Sect. A* **1976**, *32*, 751.
(34) Yang, W. J.; Luo, L. Y.; Chen, T. M.; Wang, N. S. *Chem. Mater.* **2005**, *17*, 3883.
(35) Huang, C. H.; Kuo, T. W.; Chen, T. M. *ACS Appl. Mater. Inter.* **2010**, *2*, 1395.
(36) Ruelle, N.; Pham-Thi, M.; Fouassier, C. *Jpn. J. Appl. Phys.* **1992**, *31*, 2786.
(37) Won, Y. H.; Jang, H. S.; Im, W. B.; Lee, J. S.; Jeon, D. Y. *Appl. Phys. Lett.* **2006**, *89*, 231909.
(38) Chang, C. K.; Chen, T. M. *Appl. Phys. Lett.* **2007**, *90*, 161901.
(39) Yang, W. J.; Chen, T. M. *Appl. Phys. Lett.* **2006**, *88*, 101903.
(40) Kwon, K. H.; Im, W. B.; Jang, H. S.; Yoo, H. S.; Jeon, D. Y. *Inorg. Chem.* **2009**, *48*, 11525.
(41) Paulose, P. I.; Jose, G.; Thomas, V.; Unnikrishnan, N. V.; Warrier, K. R. M. *J. Phys. Chem. Solids* **2003**, *64*, 841.
(42) Reisfeld, R.; Greenberg, E.; Velapoldi, R.; Barnett, B. *J. Chem. Phys.* **1972**, *56*, 1698.
(43) Antipeuko, B. M.; Bataev, I. M.; Ermolaev, V. L.; Lyubimov, E. I.; Privalova, T. A. *Opt. Spectrosc.* **1970**, *29*, 177.
(44) Dexter, D. L.; Schulman, J. A. *J. Chem. Phys.* **1954**, *22*, 1063.
(45) Blasse, G. *Philips Res. Rep.* **1969**, *24*, 131.
(46) You, H. P.; Zhang, J. L.; Hong, G. Y.; Zhang, H. J. *J. Phys. Chem. C* **2007**, *111*, 10657.
(47) Feldman, C. *Phys. Rev.* **1960**, *117*, 455.
(48) Liu, X. M.; Yan., L. S.; Lin, J. *J. Phys. Chem. C* **2009**, *113*, 8478.
(49) Duan, C. Y.; Chen, J.; Deng, S. Z.; Xu, N. S.; Zhang, J. H.; Liang, H. B.; Su, Q. *J. Vac. Sci. Technol., B* **2007**, *25*, 618.
(50) Xu, X. G.; Chen, J.; Deng, S. Z.; Xu, N. S.; Lin, J. *J. Vac. Sci. Technol. B* **2010**, *28*, 490.
(51) Zhang, M. C.; Wang, X. J.; Ding, H.; Li, H. L.; Pan, L. K.; Sun, Z. *Int. J. Appl. Ceram. Technol.* **2011**, *8*, 758.